ISSN-E: 2617-9563

“The Influence of Cu on the Thermal and Mechanical Properties and Microstructure of lead-free Sn–5Sb solder Alloy”

Samia E. Attia Negm

a Department of Physics, Faculty of Science, Al-Azhar Univ., Nasr City 11884, Cairo, Egypt, Girls Branch
b Department of General Science – Physics Division, Ibn Sina National College for Medical Studies, P.O. Box No. 31906, Jeddah, 21418, Saudi Arabia

ISSN-E: 2617-9563

ISSN-E: 2617-9563

Abstract

Here, we looked at how a lead-free Sn-Sb5 solder alloy's mechanical and thermal properties changed when Cu was added. Samples were subjected to differential thermal analysis (DTA) to determine their specific heat. The contact angle on different smooth-surfaced substrates (glass, pure Al, pure Cu, and CuZn30 alloy) was used to test the wettability of the molten alloys that were created. At 550K, with colophonic acid as the flux, the contact angles were photographed. The effective activation energy of Sn-Sb and Sn-Sb-Cu solder alloys was determined by conducting microhardness tests as a function of temperature. Using a constant temperature of 480 K and a pre-threshold temperature (Tm/2) for annealing, the isothermal creep curves of the alloy samples were obtained. Cold working and creep testing affect the structural changes and characteristics of Sn-Sb and Sn-Sb-Cu alloys. The effects of these treatments on the microstructure of the as-cast alloys are detailed in this study.
Keywords: Annealing temperature, Lead-Free Solder Alloy, Creep, Micro-Hardness Wetting

المستخلص:

هنا، نظرنا في كيفية تغير الخواص الميكانيكية والحرارية لسبائك اللحام Sn–Sb5 الخالية من الرصاص عند إضافة النحاس. تم إخضاع العينات للتحليل الحراري التفاضلي (DTA) لتحديد حرارتها النوعية. تم استخدام زاوية التلامس على ركائز مختلفة ذات سطح أملس (الزجاج، وAl النقي، والنحاس النقي، وسبائك CuZn30) لاختبار قابلية بلل السبائك المنصهرة التي تم إنشاؤها. عند ٥٥٠ كلفن، مع وجود حمض الكولوفونيك كتدفق، تم تصوير زوايا التلامس. تم تحديد طاقة التنشيط الفعالة لسبائك اللحام Sn–Sb وSn–Sb–Cu عن طريق إجراء اختبارات الصلابة الدقيقة كدالة لدرجة الحرارة. باستخدام درجة حرارة ثابتة تبلغ ٤٨٠ كلفن ودرجة حرارة ما قبل العتبة (Tm/2) للتليين، تم الحصول على منحنيات الزحف متساوي الحرارة لعينات السبائك. يؤثر اختبار العمل البارد والزحف على التغيرات الهيكلية وخصائص سبائك Sn–Sb و Sn–Sb–Cu. تم تفصيل تأثيرات هذه المعالجات على البنية المجهرية للسبائك المصبوبة في هذه الدراسة.

الكلمات المفتاحية: درجة حرارة التلدين، سبيكة لحام خالية من الرصاص، الزحف، ترطيب الصلابة الدقيقة

ISSN-E: 2617-9563

Introduction

Traditional soldering techniques have become essential for connecting and packaging nearly all electronic devices and circuits. Sn-Sb alloys are considered to have great potential [1]. In Sn-Sb alloys with high Sb concentrations, intermetallic compounds such as SbSn precipitates are dispersed in the matrix. This results in a significant bond strengthening effect that reduces the creep rate at temperatures below 100 °C. Most of the studies conducted in this field mainly focused on the mechanical properties of bulk solder, such as [2,3]. B. Tensile properties [4] and creep properties [5, 6]. The wetting reaction between Sn5Sb solder and Cu substrate plays an important role in the reliability evaluation of package structures. Chan et al. [1] investigated the wetting behavior of different SnSb alloys on Cu foil. Their results showed that the wetting angle decreased as the reflow time increased and varying the Sb content from 5% to 15% had no obvious effect on the wetting angle. Mechanical, electrical, and thermal properties. Sn-5Sb solder is one of the potential alternative materials to replace Pb-containing alloys [1]. The mechanical properties of the solder alloy are a crucial consideration in the design and reliability evaluation of solder connections. Thus, when it comes to the reliability of the assembly and the quality of the connection, solder selection is crucial. The mechanical features of lead-containing solders, which include low eutectic temperature, excellent wettability, low cost, high creep, and superior corrosion resistance, have made them popular for soldering in electronic applications in recent decades. [7-9] Several advantages of Sn-Cu alloy over standard Sn-Pb solder, including its low melting point, superior flowability, attractive price point, and restricted crystallization temperature range, have made it a popular choice [10,11].

The lead-free Sn-5Sb solder alloys' microstructure, melting point, heat of fusion, and creep characteristics were examined in this work. The contact angle on different smooth-surfaced substrates (glass, pure Al, pure Cu, and CuZn30 alloy) was used to test the wettability of the molten alloys that were created. At 550K, with colophonic acid as the flux, the contact angles were photographed. In order to ensure precise exposure, picture processing, and printing, a reference steel ball was utilized. Two alternative annealing temperatures were experimentally studied and discussed in relation to the creep properties of the Sn-5wt%Sb solder alloy.

Questions of the study

1. How does the addition of copper influence the thermal conductivity of the Sn–5Sb solder alloy?
2. Is there an optimal concentration of copper that maximizes both thermal and mechanical performance?
3. What advantages or disadvantages does the introduction of copper bring in terms of performance?

Objectives of the study

1. To show the influence of addition of copper on the thermal conductivity of the Sn–5Sb solder alloy.
2. To determine if there is an optimal concentration of copper that maximizes both thermal and mechanical performance.
3. To clarify the advantages or disadvantages does the introduction of copper bring in terms of performance.

Statement of the problem

As a result of regulations and worries about the environment, lead-free solder alloys are gaining popularity. The alloys with the Sn-5Sb composition have been the centre of study due to their promising qualities. But to satisfy the rigorous standards of many uses, especially in electronics, its thermal and mechanical properties must be improved. An examination of the effects of copper (Cu) on the Sn-5Sb solder alloy's microstructure, mechanical strength, and thermal conductivity is the primary objective of this study. Although copper may have some positive effects, it is not yet known how exactly these attributes will be affected. Thus, the main objective of this research is to deduce the effects of different

copper concentrations on the microstructure, thermal and mechanical properties, and lead-free Sn-5Sb solder alloy. For today's soldering applications, which place high demands on mechanical dependability and environmental friendliness, this information is vital for optimising the alloy's composition.

Significance of the study

The study addresses the ongoing need for lead-free solder alternatives, especially in electronic applications. Understanding how the addition of copper influences the thermal properties of the solder alloy is crucial for improving heat dissipation in electronic devices. and Investigating the influence of copper on the properties of Sn–5Sb solder also provides valuable insights into the development of environmentally friendly and compliant solder materials, aligning with global efforts to eliminate or reduce the use of hazardous substances in electronics.

Definition of terms

Cu (Copper): A chemical element (symbol Cu) with excellent thermal and electrical conductivity. In the context of the study, it refers to the incorporation of copper into the Sn–5Sb solder alloy.

Sn–5Sb Solder Alloy: A solder alloy composed primarily of tin (Sn) and antimony (Sb), with the numbers indicating the percentage composition of each element. In this case, the alloy consists of 95% tin and 5% antimony.

Theoretical framework

Thermal Behavior: The research employs Differential Thermal Analysis (DTA) to explore the specific heat of the alloy samples. This draws from thermodynamic principles, allowing for a detailed examination of the temperature-dependent changes in thermal properties. Understanding how Cu affects the specific heat provides valuable insights into the alloy's thermal conductivity and behavior at different temperature regimes.

Mechanical Behavior: Mechanical properties are assessed through microhardness tests conducted as a function of temperature. This approach aligns with materials science and mechanical engineering principles, providing a nuanced understanding of the alloy's hardness and how it responds to varying temperatures. The calculation of the effective activation energy further contributes to insights into the alloy's mechanical behavior under different conditions.

Wettability and Interfacial Phenomena: the study explores the wetting characteristics of the molten alloys on various substrates, utilizing contact angle measurements. This investigation integrates concepts from interfacial science and materials engineering, shedding light on the alloy's behavior at interfaces with different materials. The selection of specific substrates and the use of colophonic acid as flux introduce chemical considerations to the exploration of wettability. [36]

Creep Behavior: deformation mechanics and materials science principles underpin the investigation into isothermal creep curves. Applying constant stresses at a set temperature and subsequently annealing the samples at a pre-threshold temperature allows for a comprehensive understanding of the alloy's creep behavior. This aspect of the research is vital for applications where the alloy may experience sustained stress over time.

Microstructural Studies: the theoretical framework incorporates metallurgical principles for the analysis of microstructural changes in the as-cast alloys after annealing treatment. Investigating the influence of cold working and creep testing on the alloy's structural properties adds depth to the study.

Study limitations

While the study provides valuable insights, it is important to acknowledge certain limitations. One notable limitation is associated with the experimental conditions and their representation of real-world applications. The investigation primarily focuses on the thermal and mechanical behavior of the solder alloy under controlled laboratory conditions. This controlled environment may not fully capture the complexity of conditions the solder alloy may encounter in practical applications, where factors such as variable temperatures, diverse substrates, and dynamic stresses are prevalent.

Another limitation lies in the scope of the study, which primarily examines the influence of copper (Cu) addition on the alloy's properties. While this is essential for understanding specific compositional

effects, the study may not comprehensively address the alloy's performance in broader contexts or interactions with other alloying elements that are common in practical applications.
Furthermore, the study's focus on isothermal creep curves at a constant temperature of 480 K might not fully represent the diverse temperature conditions experienced in real-world applications. Creep behavior is critical for solder alloys in various thermal conditions, and a broader temperature range in the study could enhance the applicability of findings.
While the microstructural studies offer valuable insights, the study's limitations may include the lack of a comprehensive investigation into the alloy's long-term structural stability and reliability, which is crucial for applications requiring sustained mechanical performance.

2. Experimental

2.1Sample Preparation

The samples were crafted from extremely pure elements, specifically tin, antimony, and copper, with a weight percent purity of 99.99%. With a precision of 10−4 grammes, the sample's weight was ascertained using a delicate microbalance. To avoid sample oxidation in air and enhance mixing and melting, the weighted samples were placed in clean Pyrex tubes under a natural flux of chemical components, rosin, which also included abetic acid. To make sure the melt was evenly distributed, the sample was synthesised over the course of 20 minutes in a benzene fire while the tube was shaken. The tube was broken to obtain a large alloy after it had solidified. Excess flux was removed by soaking the billet in pure carbon tetrachloride (CCl_4) for sufficient time. The density of the prepared samples was determined by displacement method using carbon tetrachloride (CCl_4, $\rho = 1.595$ g/cm^3) as the immersion liquid. Sample density was calculated using the following formula:
(1) where, W is the weight of the sample and ρ is the density.

3. Results

3.1 Bulk Density Measurements

The value of the experimental (ρexp) bulk density for the (lead-free) low melting point binary alloys used in the present work were determined and given in Table (1). While the calculated density and the porosity percentage was calculated as follows:

ρ_{cal} = [weight percent x density element (1)]+[weight percent x density element (2)]

$$Porosity\% = 1 - \frac{\rho_{exp}}{\rho_{cal.}} \text{ x } 100 \qquad (2)$$

As shown from Table (1) the results proved that the present preparation procedure is adequate concerning these alloys.

Table 1
Densities, porosity, Melting Point, enthalpy, and Specific heat of the Sn-Sb solder alloys

Alloy	Density calculated	Density Experimental	Porosity %	M..P (K)	ΔH (cal./gm)	Specific heat	
						Temperature(K)	Cp (J/kg.K)
$Sn_{95}Sb_5$	7.1	7.03	0.01	511	5.91	450	216.7
$Sn_{94.3}Sb_5Cu_{0.7}$	7.3	7.11	0.03	490	5.42	430	223

3.2 Thermal Analysis

3.2.1 Differential Thermal Analysis (DTA) Measurements

Melting temperature is an important solder property because it determines the maximum operating temperature of the system and the minimum processing temperature that its components must withstand. The DTA results are used to obtain information about the melting or solidification behavior of the alloy. For example, liquidus and solidus temperatures are extracted from data collected during liquidus or solidus operation. Two characteristic phenomena are observed in the DTA thermogram. The first one corresponds to the melting temperature T_m and corresponds to the intersection of two straight line segments adjacent to the transition shoulder of the DTA in the endothermic direction. The second is related to the melting transition region (endothermic region). The differential thermal analysis thermograms of eutectic alloys (Sn-Sb5 and Sn-Sb5-Cu0.7) are shown in the figure. (1a, b) or Figures show the melting points of Sn-Sb and Sn-Sb-Cu alloys from Table (1).

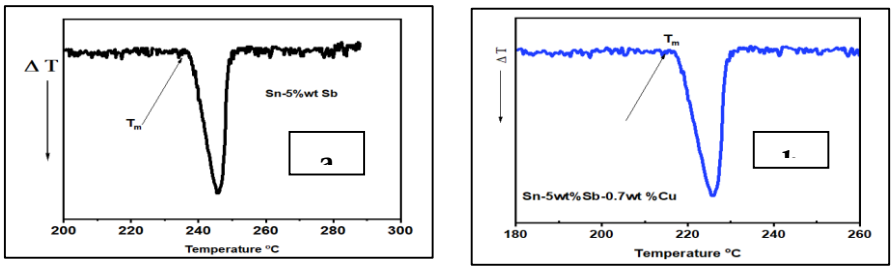

Fig. (1): The DTA thermograms of (a) Sn-Sb_5 (b) Sn-Sb_5-$Cu_{0.7}$ solder alloys.

3.2.2 Calculation of the Latent Heat of Fusion

Thermal stability was investigated by calculating the enthalpy released during the transformation process, i.e. Latent heat of fusion. Experimental evaluation of the enthalpy (ΔH) during the melting process was determined from the calibration curve of DTA by measuring the area under the DTA peak and using indium and bismuth as standards (ΔH_{ref}). Applying the formula:

$$\Delta H = \Delta H_{ref}\, A/M \qquad (3)$$

where A is the area under the DTA peak and M is the mass of the sample. The calculation results of enthalpy ΔH of Sn-Sb5 and Sn-Sb5-Cu0.7 alloy are shown in Table (1).

3.2.3 *Specific Heat Measurements*

To measure the specific heat of the samples, a Newtonian cooling experiment with Al2O3 as the reference material was used.

$$C'_p = \frac{\left[m\, C''_p \frac{dT}{dt}\right]_{Al_2O_3}}{m\left[\frac{dT}{dt}\right]_s} \qquad (4)$$

where C'_p is the specific heat of the sample, C''_p is the specific heat of Al_2O_3, m is the mass in gm and dT/dt is the temperature gradient.

A Pyrex tube (4 mm diameter) was used as a measuring cell. The tube was inserted into a vertical oven. An AC control transformer was used to control the heating current. Temperatures were recorded with an accuracy of ±0.5°C using an automatic computer circuit. The temperature of the powder sample in the oven was measured using a calibrated thermocouple (nickel-chromium type K) with a diameter of 0.07 mm placed on the measuring sample of approximately 0.17 gm to ensure a high degree of reaction. After the sample reached a high temperature of 350 °C, it was removed from the oven and cooled independently to room temperature in a large cylindrical cavity. The same procedure was performed on the same weight of Al_2O_3 powder and used as a reference sample. Several properties determine the overall effect of applying heat to a metal or alloy. For example, the specific heat Cp controls the temperature rise ΔT that results from adding a given amount of heat Q to one kilogram of metal [12.13]:

$$Q = Cp\Delta T \qquad (5)$$

The specific heat of the alloy studied is That's right. It was evaluated according to Newton's cooling hypothesis [15]. The specific heat versus temperature and temperature-time cooling curve of Sn-5wt.%Sb are shown in the figure. (2 a, b), the liquidus point is 511 ±1 K.

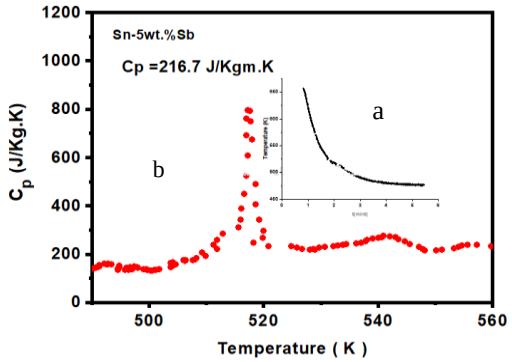

Fig. (2): a) The specific heat curves versus temperature together with b) The temperature-time cooling curves for Sn-Sb_5.

Specific heat results at selected temperatures for Sn-Sb5 and Sn-Sb5-Cu0.7 alloys from Dulong and Petit are shown in Table (1). For an alloy to be valuable as a solder in the electronics industry, it must have certain properties, such as melting range. The liquidus temperature must be low enough so that the components and circuit board are not damaged during soldering (above which they will melt completely). (5) The specific heat of the investigated alloys was evaluated according to the Newtonian cooling hypothesis [15]. The specific heat versus temperature and temperature-time cooling curve of Sn-5wt.%Sb are shown in the figure. (2 a, b), the liquids point is 511 ±1 K .

3.2.4 Wettability Measurements

Use as a filler metal in low-temperature applications is one of the most significant uses of the alloys that were examined. The conditions for wettability need to be studied. Prior to "solderability," the capacity of solder to actually create a connection on a circuit board, there is a property called "wettability" that describes the propensity of liquid metal to spread over a solid surface. One way to quantify this is by looking at the contact angle at the flux triple points or solder-substrate-air intersections [14,15]. It is also critical to correlate the alloy's microstructure with its mechanical properties (tensile strength, fatigue resistance, creep resistance) in order to optimize the joint's operating performance [16]. An objective measure of wettability is the contact angle that forms at the triple point of solder, substrate, and flux. A combination of the solder ball alloy's height, base diameter, and contact angle was used to determine the solder wettability. Here, we mimic real-world industrial circumstances by coating the solution with a flux (colophonic acid) as we make molten alloy. Photographic exposure, development, and printing were all double-checked with the help of a steel ball.

Figures (3) shows the wetting behavior of binary molten alloys prepared on different substrates (Cu, $CuZn_{30}$, Al, glass) after 60 s at a temperature of 550 K. Over time, glass substrates were chosen to resemble dielectrics. The contact angles measured from the numerical values of the used Sn-Sb5 and Sn-Sb5-Cu0.7 alloys have the values listed in Table (2). The results show that the contact angle of the alloy on Cu and CuZn30 substrates is in the range of 37–42°, suggesting that this alloy melt can be used for soldering or

Reference

s objects. Even Sn-5 wt% Sb-0.7 wt% Cu is sufficient to be considered in the development of older connections in microelectronic packaging [17].

(d) θ=119°

Fig. (3): Contact angel for (Sn-Sb_5) alloy on: (a) Cu substrate. (b) $CuZn_{30}$ substrate. (c) Glass substrate. (d) Al substrate.

Table 2

Contact angles of the alloys on different substrates after 60 s elapsed time, Room temperature Vickers hardness numbers and activation energies of the Sn-Sb solder alloys.

Alloy	Contact angles at temperature 550 K				Vickers hardness numbers	
	Glass substrate	Al substrate	Cu substrate	CuZn30 substrate	HV. at R.T. (N/mm2)	Activation energy (kJ/mole)
Sn95Sb5	116	112	39	37	135.3 ±6	5.03
Sn94.3Sb5Cu0.7	119	114	40	42	115.4 ±11	5.96

3.3 Mechanical Properties

The characteristics of the mechanical properties of a material is strength, elasticity, ductility, creep, and hardness. Each of these is associated with the ability of the material to resist mechanical forces.

3.3.1 Microhardness Measurements

Alloys can have their grain sizes, phases, and structural components microhardness tested. Here, the indentation's distorted volume can't be greater than the particle's actual volume. Consequently, the indenter is subjected to a certain amount of force [18]. A Vickers Shimadzu microhardness metre was used to assess the samples' microhardness in this study. Here, the ground or polished surface is subjected to the force of a square diamond pyramid, with opposing surfaces at an angle of 136°. An indicator of hardness is the measurement of the indentation's depth or size. The hardness index drops as the depression widens and deepens as the material's softness increases. The Vickers hardness number HV was determined using the following formula [19]: $H_V = \frac{2P\sin\frac{\alpha}{2}}{d^2} = 1.8544\frac{P}{d^2}$ (kg/mm^2) (6)

where P is the applied load and α is the angle between opposite faces of the diamond inventor (α = 136º), and d is the average length of the two diagonals of the indentation, in mm, measured, after removing the load, by means of a micrometer microscope.

Here, we measured seven distinct indentations at room temperature with an applied force of 50 g for 5 s each. We then averaged the results and determined the standard deviation. The sample surface must be meticulously prepared for indentation testing by grinding and polishing it to a clean finish. This ensures that the surface is flat and parallel. The low-load microhardness values of pure Sn, Sb, and Cu, as well as their various alloys, at room temperature were determined using Equation 6, and the results are displayed in Table (2). Below a certain indentation size, the microhardness of some materials (like metal) diminishes continuously as the load lowers, whereas it remains constant above this size. According to Buckle [20.21], the reason these materials get harder as tension decreases is because they have covalent bonding areas. The increased microhardness values at greater loads have been attributed to many factors. At low loads, the indentation size approaches the length of the sliding strip at equivalent strain, and the hardness value

increases, according to McClintock and Argon [22]. In addition, at the same strain levels, cold-worked metals usually have a lower dislocation density, but the imprint's strain gradient could make that unnecessary. At larger loads, the work hardening that polishing introduces into the surface can become significant, as pointed out by Meyers and Chawla [23]. Although inadequate elastic recovery is typically insignificant at larger pressures, Dieter [24] argues that it has a substantial impact on the impression under these conditions. Based on his research, Braunovic [25] concluded that the indenter-induced displacement of dislocations is the mechanism by which indentation hardness is load dependent. A punching mechanism can be described as the cause of dislocation creation on the contact surfaces. In crystalline solids, lattice imperfections including grain boundaries, vacancies, solutes, precipitates, and similar structures can obstruct and trap dislocations, making this movement more difficult.

3.3.2 Hot Hardness

When testing heat-stable and heat-resistant structural materials, it is crucial to determine their hardness during heating, also known as high temperature hardness measurement. Some of the things that might influence these metrics are: The measured hardness can be greatly affected by the localised cooling generated by the cold indenter, which in turn affects the precision of the results. The presence of oxidation on the surface of the sample might also lead to substantial mistakes. The process of oxidation intensifies with increasing temperature when exposed to an oven without a protective environment [18]. As a metal heats up, its ions, not its valence electrons, soak up all the energy, causing their vibrational amplitude to increase. The metal softens and opens up as the crystal reaches a new equilibrium ionic distance, the distance between atoms that bonding forces act upon rises, and the crystal expands [26]. Eventually, bonding forces are unable to maintain cohesiveness due to the increasing temperature and increasing distance, and the metal melts. Cohesion and toughness are both enhanced by a high melting point. In the image, we can see the temperature-dependent link between the Vicker hardness numbers for the Sn-Sb5 and Sn-Sb5-Cu0.7 alloys, as determined by Eqn. (7). (4a and b). From the figure, adding a small amount of Cu to Sn-Sb increases the Vicker hardness and improves the mechanical properties compared to pure Sn and Sb elements. An exponential fall in microhardness is observed as the alloy temperature increases. As a result, its mechanical characteristics and wear resistance can be diminished when heated.
An Arrhenius equation describe the obtained results quite well and is given as:

$$H_V(T) = H_{Vo} \exp(Q/kT) \qquad (7)$$

The hardness under thermal conditions is denoted as HV(T), the initial state hardness is denoted as HVo, k is the Boltzmann constant, and Q is the activation energy linked to thermal softening of the material.
We used the figure's data to calculate microhardness by plotting the logarithm of the hardness. Figure 5a and b indicate that, according to Eqn. (7), a straight line would be formed for alloys when plotting values against the reciprocal of the absolute temperature (5a and b). The Table summarizes the results of calculating the softening activation energy Q of pure metals and their alloys from the slope of these straight lines. (2).

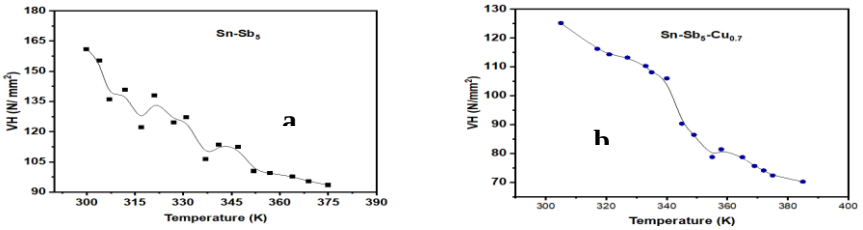

Fig. (4): The relation between the Vicker hardness number as a function of temperature for (a) $Sn\text{-}Sb_5$ and (b) $Sn\text{-}Sb_5\text{-}Cu_{0.7}$ alloys

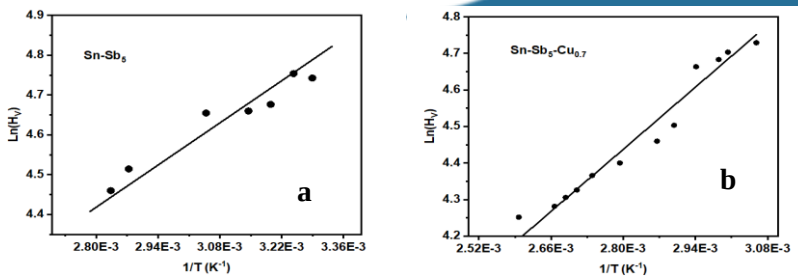

Fig. (5): Variation of the Vickers hardness number as a function of (1/T) according to Arrhenius equation for

a) Sn-Sb_5 and b) Sn- Sb_5-$Cu_{0.7}$ alloy.

3.3.3 Creep Results

Modern technological advances require materials to be used at higher temperatures. One of the most important factors when considering such applications, and perhaps one of the most important, is creep behavior. The traditional method to study this creep is to subject a tensile sample to a constant load at a constant high temperature T and record its elongation ε versus time t. In some cases, the load may be automatically adjusted during stretching so that the average stress σ remains constant across the reduced section. This adjustment has limited value because it can hardly compensate for the variations in stress and strain at different points within the deforming grain [14]. Sn-Sb5 and Sn-Sb5-Cu0.7 creep samples were fabricated in the form of ribbons using melt-spinning technique (to obtain ribbons with good shape, the surface speed of the aluminum wheel was approximately 18.65 m/s). The rapid melt-spun ribbon samples were first annealed at 440 ± 2 K for 1 hour. The creep curves of rapid melt-spun ribbon Sn-Sb and Sn-Sb-Cu alloys were obtained at constant test temperature and different stress are shown in the figure. (6a,b). The creep process under constant load is highly temperature dependent. The observed creep behavior has three characteristic stages. The creep process consists of three distinct regions: an unstable first one where the rate of creep fluctuates quickly, a steady-state creep zone where the rate of creep stays constant, and a third region where the rate of creep grows rapidly, leading to failure. The standard sort of creep behaviour was observed at each stress level, which means that there was an initial increase in strain (□o), a subsequent decrease in strain rate (primary creep), and finally, a lengthy period of secondary creep at a constant strain rate. the last one, tertiary creep. According to this naming scheme, there are four phases to a creep curve, with instantaneous strain being the initial step [27]. Such behaviour is common in several creep alloys belonging to the M-class and in pure metals as well. Class M creep behaviour was seen in the solid solution reinforced alloy, which is explicable given that prior analyses demonstrated that stress levels were high enough to permit dislocations from the resistance of solute atoms [28]. The main factors that dictate creep characteristics are microstructure, composition, and temperature. Figures (6a and b) display the microstructures of Sn-Sb and Sn-Sb-Cu alloys following creep tests. The elongation of the grains compared to prior creep testing indicates the influence of deformation on the microstructure of alloys with high grain diameters. Testing the alloy's creep behaviour up to its melting point revealed that melting had little effect on the alloy's creep behaviour. The microstructure of this alloy was thought to be responsible for its erratic creep behaviour. Figure 7 shows the plot of the strain rate vs. for Sn-Sb as an example, and it provides an indicator for the three stages: transient, steady-state, and tertiary. As a material experiences creep strain and time, its internal structure changes, leading to variations in strain rates, also known as creep rates.

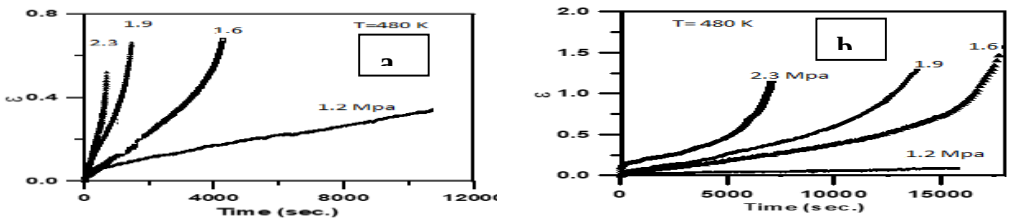

Fig. (6): Isothermal creep curves under different stress and annealing temperature (440±2K) for (1 hr) for
(a)Sn-Sb and b) Sn-Sb-Cu solder alloys in ribbon form.

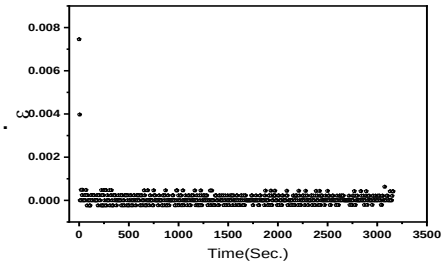

Fig. (7): The differential creep curves for $Sn\text{-}Sb_5$ solder.

3.3.4 Microstructure of the as Cast Alloys

Microstructural analysis of solder alloys reveals significant compositional and processing-related changes between the two alloys examined (Sn-Sb5 and Sn-Sb5-Cu0.7). Applying an etching reagent to a metallographic sample's polished surface selectively destroys the structure from the surface downward, making structural features partially apparent. Because various etching chemicals are usually used to address the various components of a multiphase alloy or the cut planes of differentially oriented grains of a pure metal or single-phase alloy, this form of portrayal of metal structures is possible. Its high disintegration rate is the reason behind this. In addition to presenting structural details by preferential breakdown, the active property of certain reagents is to selectively discolour or stain certain phases of the structure [29]. Microstructural alterations and the introduction of novel intermetallic compounds (IMCs) into the matrix alloy can often enhance strength while decreasing ductility [30]. The microstructure of a copper solder-copper junction that was formed under the same circumstances as the lead-free SnSbCu solder was melted and solidified, as well as the interface between a copper substrate and the solder after wetting at 623 K and 1800 s. We conducted joint research on this occurrence [31]. Figure (8a) shows, under magnification (500x), the microstructure of the as-cast Sn-Sb5 alloy following an annealing temperature of 440 □2 K. Because of the unusual way the precipitated phase grows when the alloy solidifies between the liquidus and solidus temperatures, the solidified phase typically takes the shape of big particles.

a

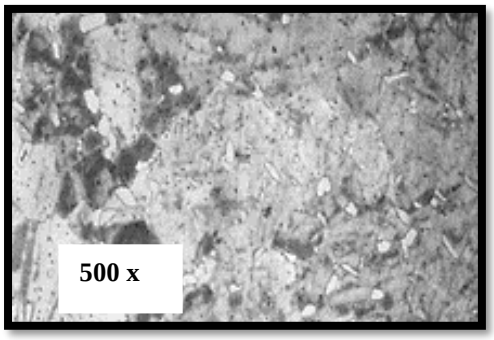

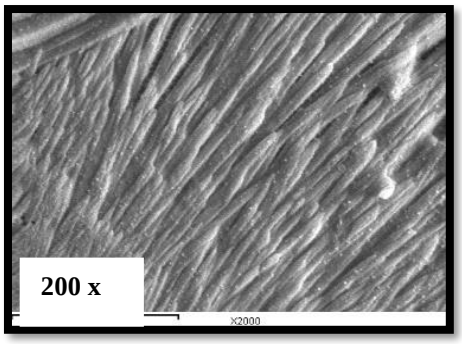

b

Fig. (8): Microstructure of (a) Sn-Sb_5 and (b) Sn-Sb_5-$Cu_{0.7}$ as-cast after annealing at 440 ± 2 K for 1 hr.

Figure (8b) shows the microstructure of the Sn-Sb5-Cu0.7 alloy in its original as-cast condition following an hour of annealing at a temperature of 440 □2 K. Through the examination of micrographs, it has been determined that this alloy is composed of almost pure Sn, intermetallic Ag3Sn in the form of rods or a dendritic eutectic mixture inside a pure Sn matrix, and intermetallic Ag3Sn phases within a pure Sn matrix. [32]. You can change the dendritic eutectic mixture's form by adjusting the annealing temperature. A layered two-phase eutectic structure of Sn parent and intermetallic compound Cu3SnSb phases makes up the area between the Sn dendrites. In figure (8), we can see the bulk sample's structure following the annealing temperature of (440 ±2 K). Before the creep test, the construction is shown in figure (8) at an annealing temperature of (440 ±2 K)for one hour, following cold work. Dendrites were aligned and broken along lines due to cold deformation. Metallographic micrograph of Sn-Sb5 alloy crawling under stress (2.3 MPa) at 480 K test temperature (500x magnification) is also shown in Figure (8a). Although the structure is lower in orientation following tensile deformation, it still retains β-Sn dendrites oriented along the tensile axis. The elongation of the grains compared to before the creep test in Figure (8a) indicates the influence of excessive deformation following the creep test on the microstructure of the alloy, which becomes more apparent with very large ingot sizes. Figure (8b) (200x magnification) shows the metallographic micrograph of the eutectic Sn-Sb5-Cu0.7 alloy prior to the creep test, which had a cold deformation of 94.5% at an annealing temperature of (440 ±2 K). In order to create thin plates, the crystal lattice is deformed and the initial blocks of equiaxed particles are broken.

Cold worked Sn-Sb5 alloy microstructure is shown in Figure (9a). Deformation caused the alloy's structure to undergo noticeable grain coarsening during creep at a tension of 2.3 MPa, which occurred after an annealing temperature of (440 ±2 K) [23]. Because of the dissolution or segregation of Sn-Sb intermetallic compounds and grain boundaries, the density of Sn-Sb intermetallic particles in the matrix was also lowered. Figure (9b) shows that the shape of the crystal grains changes when deformation occurs as a result of the creep test. Under stress (2.3 MPa) and test temperature 480 K, the microstructure of the Sn-Sb5-Cu0.7 eutectic sample crept as shown in Figure (9b), 200x magnification. The creation of dislocation clusters at grain and phase borders could explain the observed drop in grain size. There are still two phases in the system, the β phase (the Sn-rich phase) and the creep temperature, which is in the two-phase area. phases, one of which is rich in lead and the other in copper. As previously demonstrated [34], this can lead to a reduction in particle diameter and break the continuity of the boundary [33]. Because of its significantly lower hardness compared to the eutectic structure, the pure Sn phase can cause creep failure if its distribution is not uniform. Additionally, the existence of Sn dendrites suggests that the sample was prepared using a non-equilibrium cooling rate [35]. Grain growth becomes more pronounced at higher temperatures in alloys that have undergone (primary) recrystallization to produce a fine-grained structure. A significant amount of primary grains was consumed and extremely big secondary grains were produced by this mechanism, which entailed the quick moving of the borders of certain recrystallized grains. Discontinuous grain growth and anomalous grain growth are other terms for the same thing [7].

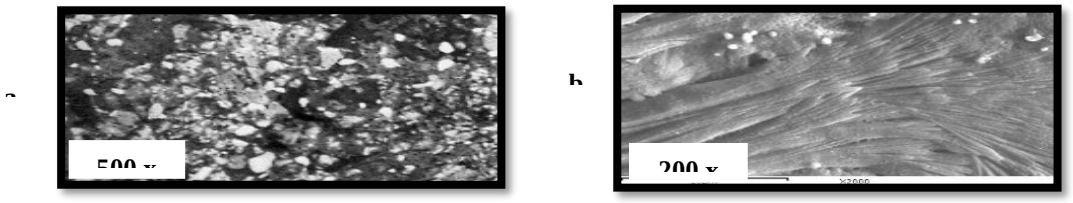

Fig. (9): Microstructure after creep for a)Sn-Sb b) Sn-Sb-Cu

Conclusion

In this study, two low melting point alloys, consisting of alloys Sn-Sb5 and Sn-Sb5-Cu0.7, were melted with weighed sample components in a Pyrex tube under a flux (colophonic acid) to prevent melt oxidation in air. Home-made computer-based circuits for differential thermal analysis (DTA), latent heat of fusion, specific heat, and creep were used for measurements. The results can be summarized as follows:

The melting points of solder alloys (Sn-Sb) and (Sn-Sb-Cu) were determined using both differential thermal analysis (DTA) measurements and specific heat.

From the DTA measurements, the heat of fusion (ΔH) during the melting process was calculated and the values for the alloy were 5.91 and 5.42 cal/g.

The specific heat of two binary tin alloys according to the Dulong-Petit criterion increases with temperature.

Wetting contact angles of three alloys were measured as droplets on various smooth substrates. The results show that the contact angles on Cu and CuZn30 substrates range from 37° to 42°, while those on Al and glass substrates range from 112° to 119°. This means that the alloy melt can be used for soldering and plating brass products.

Microhardness measurements at room temperature were calculated to be 115.4 ±11 N/mm^2 and 135.3 ±6 N/mm^2 for Sn-Sb5 and Sn-Sb5-Cu0.7 alloys, respectively. Additionally, the microhardness measurements can be fitted to an Arrhenius function (ln HV vs. 1/T) with temperature, and the thermally activated softening.

energies are 5.96 and 5.03 kJ/mol for Sn-Sb5 and Sn-Sb5-Cu0.7

Isothermal creep curves were measured for Sn-Sb5 and Sn-Sb5-Cu0.7 at a constant temperature of 480 K and different stresses ranging from 1.2 to 3.2 MPa. The creep behavior observed at each stress level was normal at four different stages.

The microstructures of the original as-cast Sn-Sb5 and Sn-Sb5-Cu0.7 alloys appear as a lameller two-phase and globular structures, respectively, after an annealing temperature of 440 K. After the creep test of Sn-Sb5 alloy, the block size becomes much larger and the grains are more elongated than before the creep test.

After the creep test, the micrographs of the Sn-Sb5-Cu0.7 alloy show that the grain size has decreased, the border continuity has been disrupted, and grain cleavage has occurred. Based on what we can see in the microstructure of as-cast Sn-Sb5 alloys, the precipitated phase typically solidifies into big grains of the alloy while the temperature stays somewhere in the solidus region. Grains of the alloy heated to the higher annealing temperature were found to be coarser in the comparison of microphotographs taken after the two temperatures. At 95% Tm, irregular and discontinuous grain development were readily apparent after cold working at a high annealing temperature (before to the creep test), which altered the grain size and shape. Grain boundary segregation or dissolution of SnSb intermetallic compounds at low annealing temperatures caused the density of Sn-Sb intermetallic particles in the matrix to drop after the creep test. Grain shape changed during high-temperature annealing.

Funding

This research received no external funding.

Declaration of competing interest

The author declares that she hasn't known competing financial interests or personal relationships that could have appeared to influence the work reported in this paper.

References

[1] El-Taher, A. M., Abd Elmoniem, H. M., & Mosaad, S. (2023). Influence of Rotating Magnetic Field (RMF) on Dendrite Growth, Mechanical and Elastic Properties of Sn-Cu-Co Lead-Free Solder Alloy. Arab Journal of Nuclear Sciences and Applications, 56(4), 141-151.
[2] Chen, S. W., Chen, P. Y., & Wang, C. H. (2006). Lowering of Sn− Sb alloy melting points caused by substrate dissolution. Journal of electronic materials, 35, 1982-1985.
[3] McCabe, R. J., & Fine, M. E. (2002). Creep of tin, Sb-solution-strengthened tin, and SbSn-precipitate-strengthened tin. Metallurgical and Materials Transactions A, 33, 1531-1539.

[4] Mahmudi, R., Geranmayeh, A. R., & Rezaee-Bazzaz, A. (2007). Impression creep behavior of lead-free Sn–5Sb solder alloy. Materials Science and Engineering: A, 448(1-2), 287-293.

[5] Kerr, M., & Chawla, N. (2004). Creep deformation behavior of Sn-3.5 Ag solder at small length scales. Jom, 56, 50-54.
[6] Joo, D. K., Yu, J., & Shin, S. W. (2003). Creep rupture of lead-free Sn-3.5 Ag-Cu solders. Journal of electronic materials, 32(6), 541-547.

[7] Huang, H., Chen, B., Hu, X., Jiang, X., Li, Q., Che, Y., ... & Liu, D. (2022). Research on Bi contents addition into Sn–Cu-based lead-free solder alloy. Journal of Materials Science: Materials in Electronics, 33(19), 15586-15603.

[8] Xu, L., Chen, X., Jing, H., Wang, L., Wei, J., & Han, Y. (2016). Design and performance of Ag nanoparticle-modified graphene/SnAgCu lead-free solders. Materials Science and Engineering: A, 667, 87-96.

[9] El-Daly, A. A., El-Taher, A. M., & Gouda, S. (2015). Novel Bi-containing Sn–1.5 Ag–0.7 Cu lead-free solder alloy with further enhanced thermal property and strength for mobile products. Materials & Design (1980-2015), 65, 796-805.

[10] Ghosh, A., & Mandal, K. (2014). Effect of structural disorder on the magnetocaloric properties of Ni-Mn-Sn alloy. Applied Physics Letters, 104(3).

[11] Osório, W. R., Spinelli, J. E., Afonso, C. R., Peixoto, L. C., & Garcia, A. (2011). Microstructure, corrosion behaviour and microhardness of a directionally solidified Sn–Cu solder alloy. Electrochimica Acta, 56(24), 8891-8899.

[12] Guy, A. G. (1974). Elements of physical metallurgy. (No Title).

[13] Kumaraswamy, J., Kumar, V., & Purushotham, G. (2021). A review on mechanical and wear properties of ASTM a 494 M grade nickel-based alloy metal matrix composites. Materials Today: Proceedings, 37, 2027-2032.

[14] Wood, W. A. (2014). The Study of Metal Structures and Their Mechanical Properties: Pergamon Unified Engineering Series. Elsevier.

[15] Mahidhara, R. K., Sastry, S. M. L., Jerina, K. L., Turlik, I., & Murty, K. L. (1994). Room temperature tensile properties of Sn-5% Sb solder. Journal of materials science letters, 13, 1387-1389.

[16] Vianco, P. T., & Rejent, J. A. (1999). Properties of ternary Sn-Ag-Bi solder alloys: Part II—Wettability and mechanical properties analyses. Journal of Electronic Materials, 28, 1138-1143.

[17] Mahidhara, R. K., Sastry, S. M., Turlik, I., & Murty, K. L. (1994). Deformation and fracture behavior of Sn-5% Sb solder. Scripta Metallurgica et Materialia;(United States), 31(9).

[18] Geller, Y. A., & Rakhshtadt, A. G. Science of Materials,‖ Mir Publishers, Moscow, 1977. P138.

[19] Nutting, J. (1980). Engineering physical metallurgy and heat treatment by Yu. Lakhtin. Acta Crystallographica Section B: Structural Crystallography and Crystal Chemistry, 36(10), 2509-2510.

[20] Gupta, M. (2021). Introduction to metal matrix composite materials: An introduction.

[21] Bückle, H. (1959). Progress in micro-indentation hardness testing. Metallurgical reviews, 4(1), 49-100.

[22] Virk, I. S., Winnicka, M. B., & Varin, R. A. (1990). Dependence of vickers microhardness on load in the L12 titanium and zirconium ternary trialuminides. Scripta metallurgica et materialia, 24(11), 2181-2185.

[23] Meyers, M. A., & Chawla, K. K. Mechanical metallurgy: principles and applications. (No Title).

[24] Dieter, G. E., & Bacon, D. (1976). Mechanical metallurgy (Vol. 3, pp. 43-53). New York: McGraw-hill.

[25] EL-Bahay, M. M., El Mossalamy, M. E., Mahdy, M., & Bahgat, A. A. (2003). Study of the mechanical and thermal properties of Sn–5 wt% Sb solder alloy at two annealing temperatures. physica status solidi (a), 198(1), 76-90.

[26] Zeng, G., McDonald, S. D., Gu, Q., Terada, Y., Uesugi, K., Yasuda, H., & Nogita, K. (2015). The influence of Ni and Zn additions on microstructure and phase transformations in Sn–0.7 Cu/Cu solder joints. Acta Materialia, 83, 357-371.

[27] Dieter, G. E. (1988). GE Dieter. Mechanical Metallurgy. Mc Graw-Hill Book Co., New York 1986. XXIII+ 751 p., DM 138.50, ISBN 0–07–016893–8. Cryst Res Technol, 23, 194.

[28] Davidson, M. J., Biberger, M., & Mukherjee, A. K. (1992). Creep of niobium and solid solution strengthened Nb-1wt.% Zr. Scripta Metallurgica et Materialia;(United States), 27(12).

[29] Wang, C. T., He, Y., & Langdon, T. G. (2020). The significance of strain weakening and self-annealing in a superplastic Bi–Sn eutectic alloy processed by high-pressure torsion. Acta Materialia, 185, 245-256.

[30] Ghosh, M., Gunjan, M. K., Das, S. K., Kar, A., Ghosh, R. N., & Ray, A. K. (2010). Effect of Mn on Sn–Ag–Cu ternary lead free solder alloy–Cu assembly: a comparative study. Materials Science and Technology, 26(5), 610-614.

[31] Šebo, P., Švec, P., Janičkovič, D., Illeková, E., & Plevachuk, Y. (2011). Interface between Sn–Sb–Cu solder and copper substrate. Materials Science and Engineering: A, 528(18), 5955-5960.

[32] Flanders, D. R., Jacobs, E. G., & Pinizzotto, R. F. (1997). Activation energies of intermetallic growth of Sn-Ag eutectic solder on copper substrates. Journal of Electronic Materials, 26, 883-887.

[33] Tang, Y., Luo, S. M., Huang, W. F., Pan, Y. C., & Li, G. Y. (2017). Effects of Mn nanoparticles on tensile properties of low-Ag Sn-0.3 Ag-0.7 Cu-xMn solder alloys and joints. Journal of Alloys and Compounds, 719, 365-375.

[34] El-Daly, A. A., Swilem, Y., & Hammad, A. E. (2009). Creep properties of Sn–Sb based lead-free solder alloys. Journal of Alloys and Compounds, 471(1-2), 98-104.

[35] McCormack, M., & Jin, S. (1994). Improved mechanical properties in new, Pb-free solder alloys. Journal of electronic materials, 23, 715-720.

[36] Le Han, D., Shen, Y. A., He, S., & Nishikawa, H. (2021). Effect of Cu addition on the microstructure and mechanical properties of In–Sn-based low-temperature alloy. Materials Science and Engineering: A, 804, 140785.